Cosmogenic 10Be production records reveal dynamics of geomagnetic dipole moment (GDM) over the Laschamp excursion (20-60 ka)

Quentin Simon, Nicolas Thouveny, D.L. Bourles, Jean-Pierre Valet, Franck Bassinot

Earth and Planetary Science Letters 550 (2020) 116547

Contents lists available at ScienceDirect

Earth and Planetary Science Letters

www.elsevier.com/locate/epsl

Cosmogenic ^{10}Be production records reveal dynamics of geomagnetic dipole moment (GDM) over the Laschamp excursion (20–60 ka)

Quentin Simon [a,*], Nicolas Thouveny [a], Didier L. Bourlès [a], Jean-Pierre Valet [b], Franck Bassinot [c]

[a] CEREGE UM34, Aix Marseille Univ, CNRS, IRD, INRAE, Coll France, 13545 Aix en Provence, France
[b] Institut de Physique du Globe de Paris, Sorbonne Paris-Cité, Université Paris Diderot, UMR 7154 CNRS, Paris, France
[c] LSCE, UMR8212, LSCE/IPSL, CEA-CNRS-UVSQ and Université Paris-Saclay, Gif-Sur-Yvette, France

ARTICLE INFO

Article history:
Received 17 February 2020
Received in revised form 16 July 2020
Accepted 21 August 2020
Available online xxxx
Editor: M. Ishii

Keywords:
Laschamp excursion
authigenic ^{10}Be/^{9}Be ratio (Be ratio)
relative paleointensity (RPI)
lock-in depth
geomagnetic dipole moment (GDM)
atmospheric ^{10}Be production

ABSTRACT

Documenting accurately amplitude and rhythms of geomagnetic variations is a prerequisite to understand the mechanisms triggering geomagnetic excursions and reversals. We present new authigenic ^{10}Be/^{9}Be ratio (Be ratio) results covering the 60–20 ka time interval from equatorial core MD05-2920. The most significant Be ratio peak is located 18 cm above the main relative paleointensity (RPI) minimum recorded in this sequence. These are interpreted as two independent recordings of the geomagnetic dipole moment (GDM) decrease linked to the Laschamp excursion dated at *ca* 41 ka. The stratigraphic offset is assignable to post-depositional magnetization lock-in processes resulting in time delay of 1.6 ka. The Be ratio and RPI records show comparable asymmetric behavior before and after the dipole low. The Be ratio record is combined with three other series to construct a global record of ^{10}Be paleoproduction variations. This compilation demonstrates the strong coherence of low and mid latitudes data sets and its comparison with ^{10}Be-flux records from polar regions fully supports the hypothesis of a global atmospheric ^{10}Be production doubling during the Laschamp. The Be ratio stack is converted in terms of GDM using both a theoretical model and a reconstruction of GDM values using absolute paleointensities measured on lava flows. Both methods provide similar results. The dipole moment record derived from this approach ($BeDM_{20-60}$) shows the following characteristics: high field values ($> 11 \times 10^{22}$ Am^2) prior to a sharp two-steps dipole decrease until reaching minimum values ($1.8 \pm 0.7 \times 10^{22}$ Am^2) between 41.6 and 40.9 ka at the time of the Laschamp excursion. The GDM partly recovers up to values of $\sim 6.3 \times 10^{22}$ Am^2, and oscillates in this range, without showing any sharp decreases that could be associated with excursions reported within the 38–20 ka time interval (e.g. the Mono Lake excursion).

1. Introduction

The Earth magnetic field is characterized by a large fluctuations spectrum, ranging from paleosecular variation to polarity excursions and reversals. The anomalous paleomagnetic directions that strictly identify excursions are carried by paleomagnetic vectors of weak intensities, “fossilizing” weak geomagnetic field vectors, generated by a low dipole moment (e.g. Roberts et al., 2013; Channell et al., 2020). Therefore, paleomagnetic excursions can be interpreted as aborted reversals, triggered by a dipole field collapse, rather than an extra-large amplitude paleosecular variation due to waxing of non-dipole sources (e.g. Valet et al., 2008). These transient states, recorded by few lava flows or by thin sediment layers, are rapidly followed by the restoration of a significant geomagnetic dipole moment (GDM), either briefly in the opposite polarity or durably in the initial polarity. The Laschamp excursion, dated at $\sim 41 \pm 1$ ka is by far the most and best documented geomagnetic excursion (see review paper by Laj and Channell, 2015). The Laschamp and Olby lava flows (Massif Central, France) carrying quasi-reversed magnetizations (Bonhommet and Babkine, 1967) later revealed weak paleointensities (Roperch et al., 1988; Laj et al., 2014). Lava flows from New Zealand dated at the same age have since shown the same characteristics (Mochizuki et al., 2006; Cassata et al., 2008; Ingham et al., 2017). Large amplitude directional variation or even excursions were also found to be associated with weak paleointensities in lacustrine and marine sedimentary sequences of the same age and from various regions (e.g. Thouveny et al., 1993, 2004; Vlag et al., 1996; Mazaud et al., 2002; Blanchet et al., 2006; Nilsson et al., 2011; Nowaczyk et al., 2012; Channell

* Corresponding author.
E-mail address: simon@cerege.fr (Q. Simon).

https://doi.org/10.1016/j.epsl.2020.116547

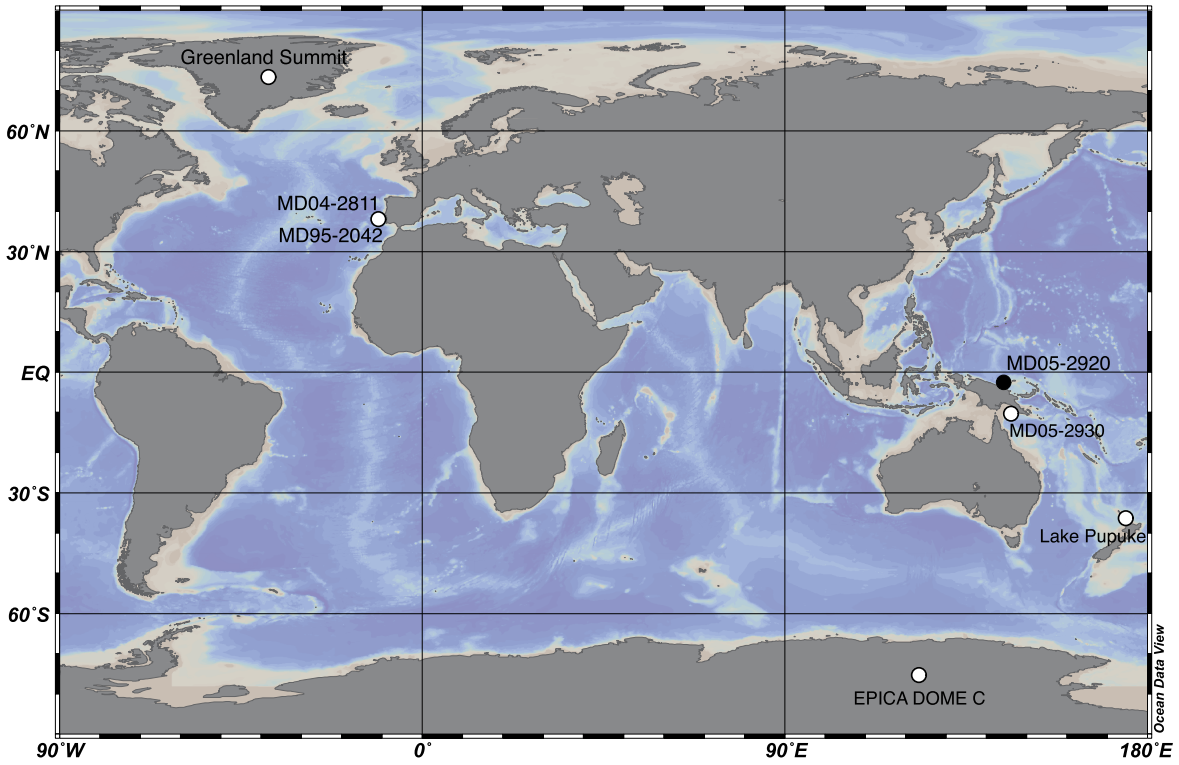

Fig. 1. Location of the studied core MD05-2920 (black dot) along with other authigenic $^{10}Be/^{9}Be$ ratio (Be ratio) and ^{10}Be flux from glacial and lake records discussed in the text. These references include Greenland Summit (Muscheler et al., 2005), EPICA Dome C (EDC; Raisbeck et al., 2017), Lake Pupuke (Nilsson et al., 2011), Portuguese margin (MD95-2042 – Carcaillet et al., 2004b); MD04-2811 - Ménabréaz et al., 2011) and core MD05-2930 from the Gulf of Papua (Simon et al., 2016a).

et al., 2017; Lund et al., 2005, 2017a). The Laschamp excursion was further identified in speleothems from North America (Lascu et al., 2016). Numerous paleomagnetic data sets of directions and paleointensities thus allow to understand the detailed structure of the Laschamp excursion and elaborate models (Leonhardt et al., 2009; Brown et al., 2018; Korte et al., 2019). However, due to several biases, such as discontinuities of lava sequences and "low fidelity" of magnetization acquisition processes, especially for relative paleointensity (RPI) reconstructions from sediments, the reliability of paleomagnetic records to capture accurate geomagnetic field dynamics is questioned, particularly during time intervals characterized by low dipole field intensities (e.g. Coe and Liddicoat, 1994; Roberts et al., 2013). Independent methods are therefore required to verify and correct for such recording biases.

The inverse relationship between GDM values and cosmogenic nuclide production rates was first proposed by Elsasser et al. (1956) and Lingenfelter (1963). It was conceptualized by Lal and Peters (1967) and first modeled and quantified by O'Brien (1979). These works led to the first measurements of cosmogenic beryllium-10 (^{10}Be) in natural archives (sediments and ice cores) to investigate the paleointensity decrease associated with polarity reversals and excursions (Raisbeck et al., 1985, 1987). The ^{10}Be is produced through spallation reactions engendered by highly energetic galactic cosmic ray particles (GCR) on the atmospheric O and N atoms. In marine sediments, the impact of deposition and environmental components on the amplitude of this production is minimized by normalizing the ^{10}Be concentrations to the concentrations of ^{9}Be beforehand dissolved through weathering processes (authigenic ^{9}Be). The authigenic $^{10}Be/^{9}Be$ ratio thus provides a robust proxy of atmospheric ^{10}Be production rates (Bourlès et al., 1989). Evidence of atmospheric ^{10}Be overproduction episodes linked to all geomagnetic excursions and reversals of the last 2 Ma have been observed in sedimentary cores (e.g. Frank et al., 1997; Carcaillet et al., 2004a; Christl et al., 2010; Simon et al., 2016a, 2018a). The detected episode of ^{10}Be overproduction at the time of the Laschamp excursion confirms, independently from paleomagnetic methods, that the GDM collapse triggered a magnetospheric shielding depletion, allowing more GCR penetration in the Earth's atmosphere (Muscheler et al., 2005; Raisbeck et al., 2017; Ménabréaz et al., 2011, 2012; Simon et al., 2016a).

In this study, we provide a new authigenic $^{10}Be/^{9}Be$ ratio (named as Be ratio hereafter) data set with an unprecedented resolution of 200 years from the west-equatorial Pacific Ocean. This new Be ratio data set compiled with three other marine sequence records allows constructing the updated global record of ^{10}Be production rate variations from 60 to 20 ka and during the Laschamp excursion. The ^{10}Be production record over the relevant time interval is then converted in terms of GDM using complementary calibration methods that provide a basis for an original discussion, independent from paleomagnetic measurements, on dipole moment field dynamics at the time of excursions and reversals.

2. Materials and methods

2.1. New sampling and Beryllium data mining

New high-resolution Be results from core MD05-2920 located in the western equatorial Pacific Ocean, on the northern coast of Papua New Guinea (2.51°S, 144.32°E, 1848 m water depth, Fig. 1) were obtained by sampling every 2 cm between 719–819 cm depth. They complete results from Ménabréaz et al. (2012) and Simon et al. (2016a) obtained with a 10 cm depth resolution. Be ratio results from core MD05-2930 retrieved from the Gulf of Papua (10.32°S, 146.73°E, 1490 m water depth), ~900 km South of MD05-2920 site (Simon et al., 2016a) are also used for stacking. The age-models of MD05-2920 and MD05-2930 sedimentary sequences are based on radiocarbon dating and correlation of the benthic foraminifera $\delta^{18}O$ to the global LR04 stack (Lisiecki and

Raymo, 2005; Tachikawa et al., 2011; Ménabréaz et al., 2014; Simon et al., 2016a). Results from core MD05-2920 are plotted on the latest chronological scale (Simon et al., 2016a) that provides an average resolution of 1 data per 200 years over the 46 to 36 ka interval straddling the Laschamp excursion, and a 500 years resolution over the rest of the 60–20 ka time interval. This improved time resolution allows accurate estimates and interpretation of the GDM variation rates over this time span. We also use Be ratio results of cores MD04-2811 (37.48°N, 10.09°W, 3162 m water depth) and MD95-2042 (37.48°N, 10.10°W, 3146 m water depth) retrieved from the same site on the Portuguese margin (Ménabréaz et al., 2011; Carcaillet et al., 2004b). The age-model of core MD95-2042 has been obtained through radiocarbon dating and high-resolution correlation of planktonic $\delta^{18}O$ to stadial-interstadial temperature changes recorded in the Greenland ice cores (Shackleton et al., 2000, 2004; Bard et al., 2004). This age-model was transferred to core MD04-2811 using magnetic susceptibility correlation (Ménabréaz et al., 2011), providing a very coherent Iberian Margin chronology. The average time resolution of these three records are 850 years (400 years over the 46–36 ka time interval) for core MD95-2042 (limited to 60–27.4 ka), 600 years (500 years over the 48–28 ka time interval) for core MD04-2811 (limited to 51–20 ka) and 1000 years for core MD05-2930. We recalculated all published Be ratio results based on original ^{10}Be and ^{9}Be data following Simon et al. (2016b) (see results in the supporting material, Tables S1-S4).

2.2. Beryllium measurements

New authigenic Be isotopes analyses were carried out at the CEREGE National Cosmogenic Nuclides Laboratory (LN2C, France) on 44 samples according to the chemical procedure established by Bourlès et al. (1989) and revised by Simon et al. (2016b). Authigenic ^{10}Be and its stable isotope ^{9}Be were extracted from 1 g dry samples by soaking them in a 20 ml leaching solution (0.04 M hydroxylamine (NH_2OH–HCl) and 25% acetic acid) at 95 ± 5 °C for 7 h. A 2 ml aliquot of the resulting leaching solution was sampled for measurement of the natural ^{9}Be concentration using a graphite-furnace Atomic Absorption Spectrophotometer (AAS) with a double beam correction (Thermo Scientific ICE 3400®). The remaining solution was spiked with 300 µl of a 9.8039×10^{-4} g.g^{-1} ^{9}Be-carrier before Be-purification by chromatography to determine accurately ^{10}Be sample concentrations from accelerator mass spectrometer (AMS) measurements of $^{10}Be/^{9}Be$ ratios at the French AMS national facility ASTER (CEREGE). ^{10}Be sample concentrations are calculated from the measured spiked $^{10}Be/^{9}Be$ ratios normalized to the BeO STD-11 in-house standard ($1.191 \pm 0.013 \times 10^{-11}$) (Braucher et al., 2015). Authigenic ^{10}Be concentrations are decay-corrected using the ^{10}Be half-life ($T_{1/2}$) of 1.387 ± 0.012 Ma (Chmeleff et al., 2010; Korschinek et al., 2010).

3. Results

The authigenic ^{9}Be concentrations vary from 1.1 to 1.7×10^{16} at.g^{-1} with an average value and standard deviation of $1.4 \pm 0.2 \times 10^{16}$ at.g^{-1} (Fig. 2B; Table S1). The narrow concentrations range and low standard deviation of ^{9}Be is associated with homogeneity of the sediments and low detrital input changes over the studied interval as shown by steady $CaCO_3$ percentages (Fig. 2A; Tachikawa et al., 2011) and by magnetic grain size proxies such as k_{ARM}/k_{LF} or $SIRM/k_{LF}$ (Fig. 2G; e.g. Stoner and St-Onge, 2007). The authigenic ^{10}Be (decay-corrected) concentrations vary from 6.0 to 15.4×10^{8} at.g^{-1} with an average value and standard deviation of $10.6 \pm 1.9 \times 10^{8}$ at.g^{-1} (Fig. 2C). The Be ratio varies from 4.3 to 12.5×10^{-8} with an average value and standard deviation of $7.5 \pm 1.7 \times 10^{-8}$ (Fig. 2D). A systematic offset of nearly 10% between the "old" ^{10}Be and ^{9}Be concentrations from Ménabréaz et al. (2012) and our new data is observed (Fig. 2B–C) and explained by different leaching durations between the two studies, since all other steps of the original method proposed by Bourlès et al. (1989) are nearly similar (Simon et al., 2016b). Most importantly, these offsets are canceled out when using the Be ratio (Fig. 2D) emphasizing the need to use the ratio between the cosmogenic radionuclide (^{10}Be) and the authigenic fraction of its stable isotope (^{9}Be) for robust interpretations of past ^{10}Be production variations, rather than comparing variations of ^{10}Be-leachate concentrations or raw ^{10}Be-fluxes (^{10}Be leachate concentrations × sediment density × sedimentation rate) that are methods dependent.

4. Be ratio and relative paleointensity (RPI) records of the Laschamp excursion

The most noticeable feature of the Be ratio in the studied interval is a peak overpassing the average value + 1 standard deviation, recorded between 756 and 784 cm depth (Fig. 2D). The corresponding RPI minimum (NRM/ARM ratio after demagnetization step at 30 mT; Ménabréaz et al., 2012) is recorded 18 cm below the stratigraphic position of the Be ratio maximum peak (Fig. 2F). Such an observation has been already realized in former studies (e.g. Carcaillet et al., 2004b; Ménabréaz et al., 2012; Horiuchi et al., 2016; Simon et al., 2018a) and explained by the delay of post-depositional remanent magnetization (PDRM), resulting in a locking-in depth modeled by several authors (e.g. Løvlie, 1976; Hyodo, 1984; Roberts and Winklhofer, 2004; Suganuma et al., 2011; Nilsson et al., 2018). These empirical and modeled estimates provide lock-in depths ranging from 0 to 30 cm. Considering that the short residence time (300 years maximum) of Be isotopes in the water column along continental margins (von Blanckenburg and Igel, 1999) represents a maximum thickness of 3 cm in the studied core, the 18 cm offset measured here can only be related to the delayed lock-in of magnetic grains before sediment compaction leading to PDRM acquisition in these clayey carbonaceous sediments. The PDRM lock-in depth varies with sediment characteristics (granulometric distribution of magnetic grains and non-magnetic matrix, organic matter content, water content, salt content) and the lock-in delay (i.e. the time needed to accumulate sediment thickness required to reach the lock-in depth) varies with sedimentation rates (e.g. Roberts et al., 2013 and references therein). The observed 18 cm lock-in depth value in core MD05-2920 corresponds to a lock-in delay of 1.6 ka. Such delay is significant compared to the short durations of RPI minima and directional anomalies linked to excursions (usually <2 ka). Furthermore, variations of the lock-in depth along a given sedimentary sequence, as well as between contemporaneous deposits imply variable delays of paleomagnetic events recording which add uncertainties on their age and duration (e.g. Sagnotti et al., 2005; Horiuchi et al., 2016; Simon et al., 2018a).

Delayed PDRM acquisition introduces other biases such as a smoothing of paleomagnetic signatures. An attenuation of the amplitude of the paleomagnetic secular variation was quantified at *ca* 20% by comparing the respective dispersions of contemporaneous populations of paleomagnetic vectors recorded in Massif Central lavas and in lac du Bouchet sediments (Thouveny et al., 1990). Theoretical approaches also showed that the PDRM intensity resulting from bioturbation processes is expected to be weaker than the DRM intensity (Egli and Zhao, 2015).

In Fig. 2E, the PDRM lock-in depth was accounted for by shifting the RPI record 18 cm upwards, providing a reasonable agreement with the Be derived dipole moment (BeDM, see section 4 for calibration methods). The two proxy records present similar asym-

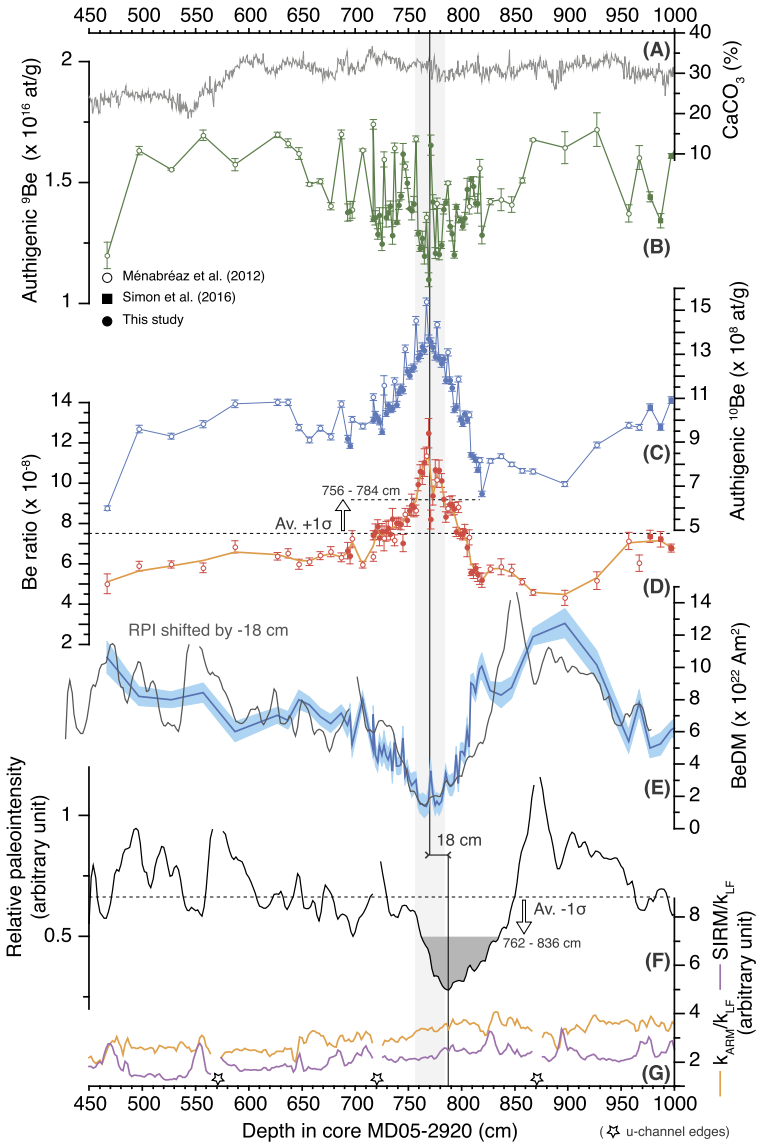

Fig. 2. Beryllium and relative paleointensity (RPI) results from core MD05-2920. $CaCO_3$ percentages (A, Tachikawa et al., 2011), authigenic ^{9}Be concentration (B), authigenic ^{10}Be concentration (C), authigenic ^{10}Be/^{9}Be ratio (D), Be ratio calibrated in term of Dipole Moment (blue, BeDM) and RPI (black, Ménabréaz et al., 2012) shifted by 18 cm to account for PDRM lock-in depth (E). RPI plotted on the core depth (F) and two rock magnetic parameters (k_{ARM}/k_{LF} and $SIRM/k_{LF}$) (G) are showned on the lower panels.

metric profiles before and after the dipole low. The RPI record however shows an earlier drop and thus a longer phase of weak field than the BeDM record that exhibits sharper variations. This difference can be due to different rates of magnetic grains (re-)alignments depending on the strength of the (re-)aligning magnetic field vector and its effects on the DRM and PDRM acquisition (shift and smoothing). Depth/time variations of the lock-in depth function thus introduce distortions of the paleomagnetic profiles (e.g. Coe and Liddicoat, 1994). Using the Hyodo (1984) model, Vlag et al. (1997) showed for instance that excursional (non-antipodal) paleomagnetic directions combined with alternatively strong-low-strong field intensities are severely smoothed and distorted by PDRM processes. This introduces variable distortions and smoothing degrees on "square shaped" synthetic declination, inclination and intensity profiles resulting in: i) downward shifts of magnetization anomalies, ii) different kurtosis and skewness of the declination, inclination and intensity profiles. These observations drawn from simple PDRM models are coherent with the results obtained for the Laschamp excursion from lacustrine sediments (i.e., Lac du Bouchet and Lac St Front, Massif central France; Vlag et al., 1996) and from the studied marine sediments (Fig. 2D). Recent paleomagnetic results and re-deposition experiments of clayey sediments further confirmed significant smearing of magnetic records due to progressive magnetic grain lock-in (Valet et al., 2016, 2017, 2019). These PDRM-related biases together with measurements on u-channels likely explain smeared/smoothed paleomagnetic directions observed in core MD95-2920, showing only moderate inclination deviations and monotonous declination variations at the time of the Laschamp.

The dependence of NRM acquisition processes on variable deposition conditions is thus the origin of biases and discrepancies of paleomagnetic records that can hamper the efficiency of high-resolution stacking. Moreover, the limited understanding of these processes can lead to different data interpretations (Roberts et al., 2013). The accuracy of the reconstructed master curves being limited, their interpretations in terms of amplitudes and rhythms of the paleomagnetic field variations should therefore be cautious to avoid introducing erroneous models of geodynamo behavior or supporting some "ad-hoc" interpretations using unreliable magnetostratigraphic correlations.

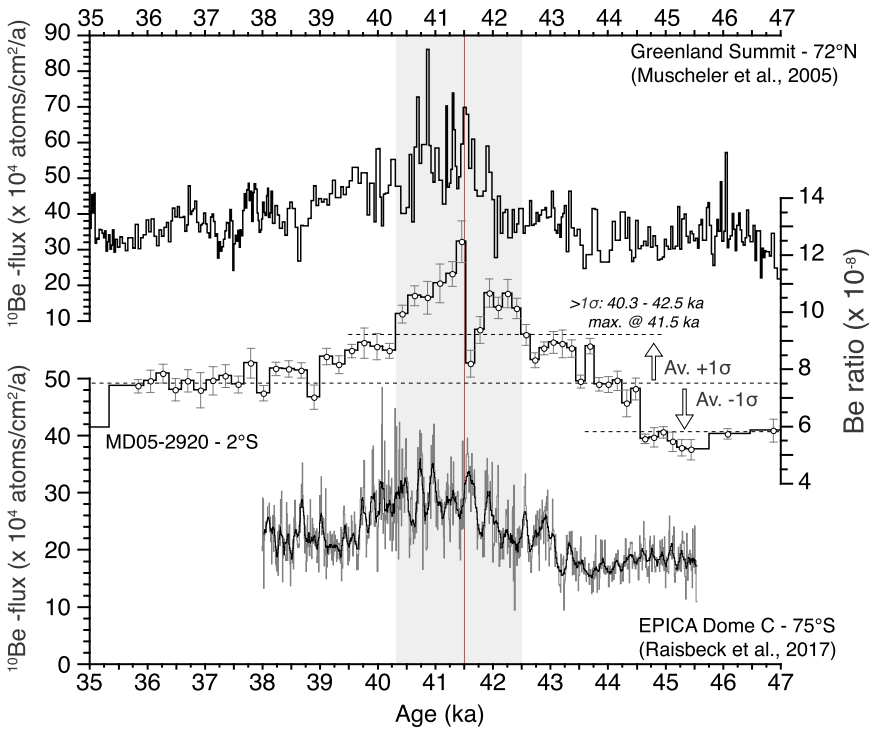

Fig. 3. Comparison of ^{10}Be production proxies over the 35–47 ka time interval between high and low latitude sites. A significant ^{10}Be overproduction signal (^{10}Be-flux in ice cores and Be ratio in marine sediments) globally synchronous is observed at the time of the Laschamp excursion (gray band).

5. ^{10}Be overproduction signature and dipole behavior during the Laschamp excursion

In Fig. 3, we compare proxy records of the ^{10}Be production covering the time interval 47–35 ka from three sites separated by 147° latitudes and 186° longitudes, i.e. ice core records from Greenland (Greenland Summit) and Antarctica (EPICA Dome C, EDC) and the equatorial marine sedimentary core MD05-2920 (Fig. 1). Due to different accumulation rates and to sampling and data treatment strategies, these archives have very different temporal resolutions. The EDC, Greenland Summit and MD05-2920 records are averaged each 10 years, ~30–50 years and 200 years, respectively, leading to different degrees of interpretations on the origins of the ^{10}Be production variations. The decadal to millennial-scale solar signals are legible in high-latitude ice core records (e.g. Beer et al., 1990; Raisbeck et al., 2017), while sediments from the equatorial site only record the geomagnetic dipole signal (Fig. 3) due to the filtering of high frequency solar modulations by i) residence time and mixing of ^{10}Be in the water column; ii) sedimentation and bioturbation processes and iii) sampling resolution. During periods of low dipole intensity, the magnetospheric shielding exerted by the non-dipole field is negligible, and the latitudinal dependency of the GCR penetration is canceled (Heikkilä et al., 2009). The ^{10}Be production increase is therefore global and homogenous.

The ^{10}Be overproduction at the time of the Laschamp excursion appears synchronous, within chronological uncertainties, at all sites (gray band in Fig. 3). In the sedimentary record the signal reveals one ^{10}Be overproduction event separated by a short amplitude drop documented by two data points (Fig. 2). The resolution of our sedimentary record does not allow further investigation and confirmation of this feature. However, a drop in the ^{10}Be production triggered by a transient restoration of a weak reversed dipole moment would be in full agreement with quasi-reversed paleomagnetic directions reported from volcanic and sedimentary recording of the Laschamp excursion (Laj et al., 2014; Nowaczyk et al., 2012). Such feature is also coherent with the structure of the atmospheric Δ^{14}C variation observed over the Laschamp interval in high-resolution records (Staff et al., 2019; Bronk Ramsey et al., 2020). Only few paleomagnetic records of the Laschamp and Iceland Basin excursions report evidence of reversed directions bound to a RPI rebound within the main low RPI interval (Roberts, 2008; Nowaczyk et al., 2012; Channell, 2006, 2014). Such RPI rebounds are rarely reported from sedimentary sequences studies, due to a lack of resolution and to PDRM smearing/smoothing (e.g. Thouveny et al., 2004; Roberts, 2008). Similarly, a short-lived and low amplitude ^{10}Be production drop associated with partial GDM recovery can be concealed by rapid lithological variations affecting available sedimentary records (Fig. 2) and likely mingled with solar modulations in high-latitude ice cores (Figs. 3 and 4A; Raisbeck et al., 2017). In most cases, the excursional declination and/or inclination signatures accompany a unique dipole low, suggesting that non-dipole sources or an equatorial dipole persist through the dipole moment low event. Such demonstration of a transient cosmogenic production decrease during the maximum production event, if confirmed would strengthen the interpretation of excursions as aborted reversals with the dipole moment vanishing, growing in the opposite polarity, and finally restoring its initial polarity (e.g. Valet and Plenier, 2008; Brown and Korte, 2016).

6. Global atmospheric ^{10}Be production variations from 60 to 20 ka

In order to produce a robust reconstruction of the atmospheric production of ^{10}Be over the 20–60 ka interval, we compiled the Be ratio records obtained from four marine sequences (Fig. 1). The Be ratio records were used on their respective time scales to produce a global stack called marine Be ratio stack (Fig. S1A). We did not attempt to fit records on one single time-series to avoid any chronological *a priori* and because the Be ratio spikes attributed to the Laschamp excursion were demonstrated to be synchronous in all cores. Time uncertainties associated with poten-

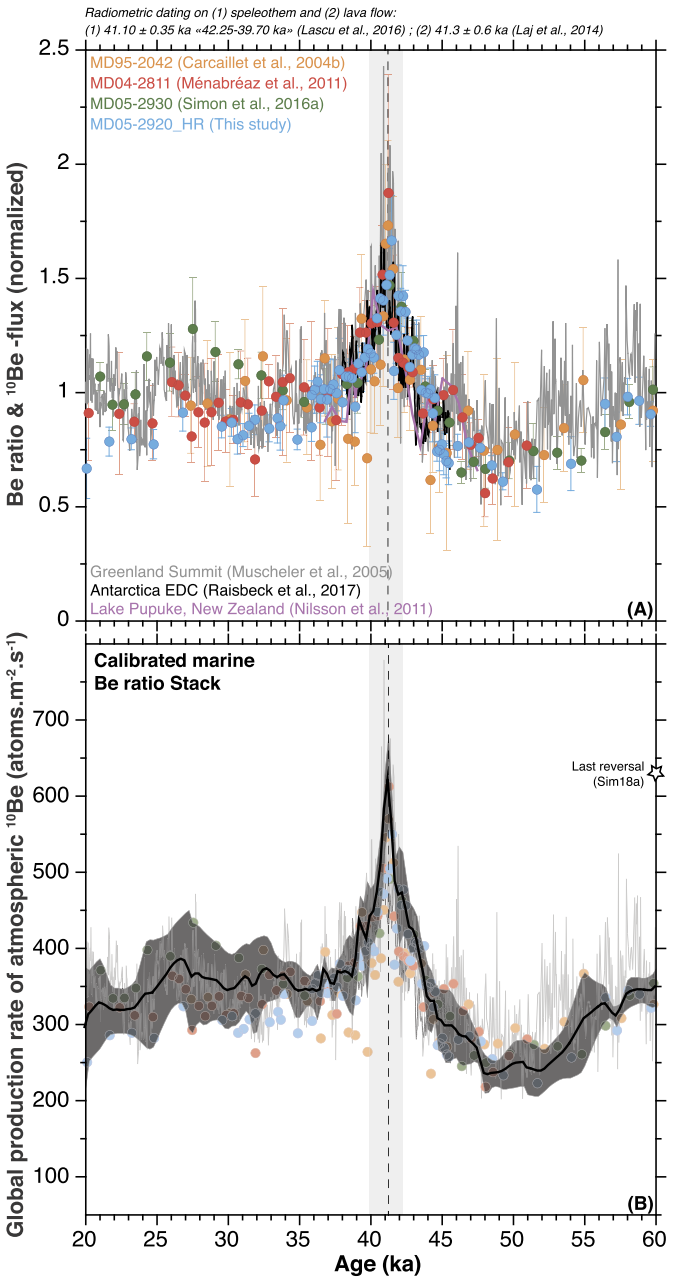

Fig. 4. Normalized Be ratio and ^{10}Be-flux dataset within the 20–60 ka time interval straddling the Laschamp excursion. (A) Normalized Be ratio from marine cores and ^{10}Be-flux from lake Pupuke and Greenland and Antarctica glacial records (see Fig. 1 for sites location). (B) Normalized Be ratio stack calibrated in terms of global ^{10}Be production rates.

tial offsets between records are therefore included within the stack itself, but are likely insignificant (<500 years). We first normalized each record to their average values to remove local influence and inter-basin variations (Frank et al., 1997) (Fig. 4A). Each normalized record was linearly re-sampled with a spacing of 250 years, which corresponds to a slight smooth of MD05-2920 record. The averaging was then performed by computing arithmetical means along each individual Be ratio record. The final uncertainty corresponds to standard deviation of the entire dataset and includes the uncertainties associated with ^{10}Be production rates and its homogenization/mixing before deposition. Outliers appear outside from the $\pm 1\sigma$ envelope (Fig. S1A). Three other stacking options were tested in order to gain resolution, but none was found satisfactory for improving the stack (see Fig. S1). A stack composed of both marine and ice-core datasets is fully consistent with the marine Be ratio stack (r=0.97, Fig. S1C), therefore, the latter was considered in order to maintain methodological coherence (marine Be ratio only) and to use an independent control using the ice records (Fig. 4B).

This compilation exhibits a high degree of internal coherence between data sets from low to mid latitudes (Fig. 1), and strong correlations with southern hemisphere ^{10}Be-flux from Lake Pupuke in New Zealand (r=0.74) and high latitude ^{10}Be-flux records from ice cores of Greenland Summit (r=0.79) and Antarctica EDC (r=0.82) (Fig. 4). This consistency supports the hypothesis of a globally synchronous atmospheric ^{10}Be overproduction provoked by a decrease of magnetospheric shielding resulting from the decrease of the Earth's magnetic field vectors produced by a weak dipole moment. This high degree of synchronization between all sites (with independent chronologies) further indicates ^{10}Be was rapidly homogenized globally by atmospheric circulation before deposition and storing in natural archives. It allows estimating accurately the ^{10}Be production at the time of the Laschamp (Fig. 4B) using the theoretical ^{10}Be production model of Poluianov et al. (2016) and transfer function of Simon et al. (2018b). The ^{10}Be production values peaked at 621 ± 60 atoms.m^{-2}.s^{-1} during the Laschamp excursion (at 41.3 ka), about two times higher than average values preceding (240–350 atoms.m^{-2}.s^{-1}) and following (350–390 atoms.m^{-2}.s^{-1}) the Laschamp time interval; and about 1.8 times higher than the present day ^{10}Be production value (e.g. Poluianov et al., 2016). Furthermore, similar ^{10}Be production values during the last reversal (638 ± 112 atoms.m^{-2}.s^{-1}; Simon et al., 2018b) and during the Laschamp excursion support the hypothesis of similar GDM amplitude collapses between aborted and successful reversals (Fig. 4B).

7. Be ratio derived geomagnetic dipole moment (BeDM)

The atmospheric ^{10}Be production being at the first order dependent on the GDM, the global ^{10}Be production curve derived from the marine Be ratio stack (see above) can be calibrated in terms of GDM using the theoretical ^{10}Be production model of Poluianov et al. (2016). An alternative approach to obtain GDM values is to calibrate the normalized Be ratio stack using absolute paleointensities (PI) compiled in the Geomagia50.v3.3 (Brown et al., 2015) and PINT2015-05 (Biggin et al., 2009) databases. While the first method is relatively straightforward (Simon et al., 2018b), the second needs preliminary requirements (e.g. Ménabréaz et al., 2011; Simon et al., 2016a, 2018a). Reliable PI are first selected from databases following strict criteria, including: i) quality of methods (only Thellier-type with pTRM checks and Shaw methods) and number of samples (N≥3) used to produce the paleointensity (PI) values from thermoremanent magnetization (TRM) component, ii) the presence of paleomagnetic directions, and iii) reasonable errors on PI (standard deviation lower than 10%) (e.g. Biggin and Paterson, 2014). This selection stage excludes extreme values associated with unreliable measurement procedures. Given the low number of reliable PI values within the studied interval (60–20 ka) and because the calibration requires a representative statistical distribution of GDM states, we used a total of 458 virtual axial dipole moment (VADM) or virtual dipole moment (VDM) data extracted from the last 2 Ma (Fig. 5A; Simon et al., 2018a). V(A)DM and normalized Be ratio averages and standard deviations are then computed within five different statistical clusters to account for uncertainties inherent to PI data and to their non-uniform distribution through time (see Simon et al., 2016a, 2018a for details). The polynomial fit between cluster averages is used to calibrate the normalized Be ratio stack. Uncertainties on the BeDM record represent the sum of standard deviations within each cluster calcu-

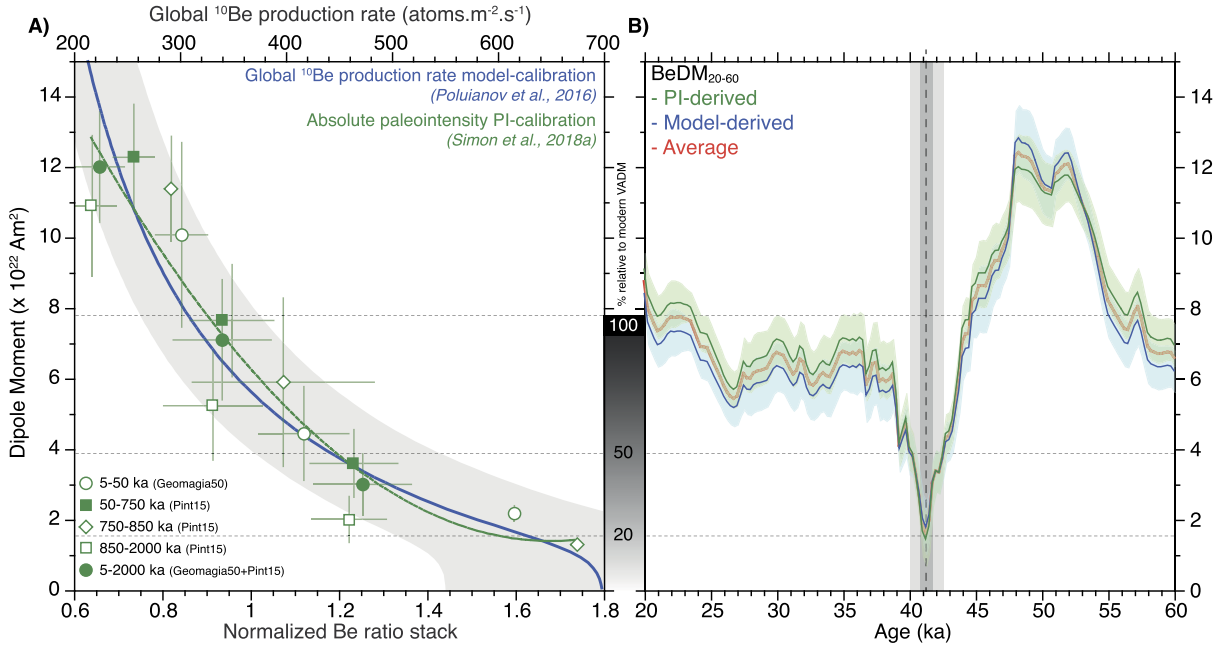

Fig. 5. Calibrations of the Be ratio stack in terms of geomagnetic dipole moment. (A) Dipole moment calibration methods. The blue line corresponds to the theoretical ^{10}Be production rates at constant mean modulation potential (550 MV) in the Poluianov et al. (2016) model. The gray shading bounds values between averages maximal and minimal modulation potentials (300–800 MV). The green symbols and polynomial fit are calculated from a selection of V(A)DM values drawn from absolute paleointensities measured on lava flows (Simon et al., 2018a). (B) Be ratio-derived dipole moment over the 20–60 ka time interval (BeDM$_{20-60}$). The blue line corresponds to a calibration using the theoretical ^{10}Be production model (Poluianov et al., 2016) and a transfer function (Simon et al., 2018b). The green line is calculated using the polynomial function from the PI calibration. The red thick line corresponds to the average between the two calibration outputs. BeDM uncertainty in Fig. 6 adds up individual uncertainties from the two methods (blue and green shades).

lated in quadrature. These two calibration methods provide similar results within error intervals (Fig. 5; Table S5).

8. Amplitude and dynamics of GDM variations before, during and after the Laschamp

We use hereafter average values and full uncertainties from the two calibration outputs (BeDM$_{20-60}$) to discuss the amplitude and dynamics of GDM variations within the studied time interval (Fig. 6). The dipole moment increases from 6.6 ± 0.8 to $8.2 \pm 0.9 \times 10^{22}$ Am^2 between 60 and 55 ka, then rises abruptly until 52 ka. From 52 to 48 ka, the dipole moment is rather stable at $11.9 \pm 0.4 \times 10^{22}$ Am^2 which corresponds to about 150% of the present-day dipole moment value. These values are compatible with high-resolution calibrated-RPI stacks such as GLOPIS-75 (based on marine cores with sedimentation rates >7 cm/ka), but are significantly higher than those obtained from geomagnetic models (Fig. 6) or from the PADM2M model incorporating absolute PI and RPI data through penalized maximum likelihood spline fit (Ziegler et al., 2011). Similar discrepancies are observed on dipole field intensities for overlapping periods between models using archeomagnetic data only, models using mixed archeomagnetic and sedimentary data and compilation of absolute PI data (e.g. Genevey et al., 2008; Knudsen et al., 2008; Pavón-Carrasco et al., 2014; Korte et al., 2011). They may be assigned to i) analytical smoothing inherent to data regularizations and propagation of uncertainties in models; ii) transfer of energy from the dipole component to higher-order components to reduce the misfit between data and the modeled field; and/or iii) impact of the PDRM smearing on sedimentary paleointensity records. Furthermore, the BeDM$_{20-60}$ record being only dependent on dipole field, a hypothetical impact from regional non-dipole components can be ruled out.

From 48 to 41.3 ka, the GDM collapsed from 12.3 ± 1.0 to $1.6 \pm 0.7 \times 10^{22}$ Am^2 (average falling rate of -1.6×10^{22} Am^2/ka).

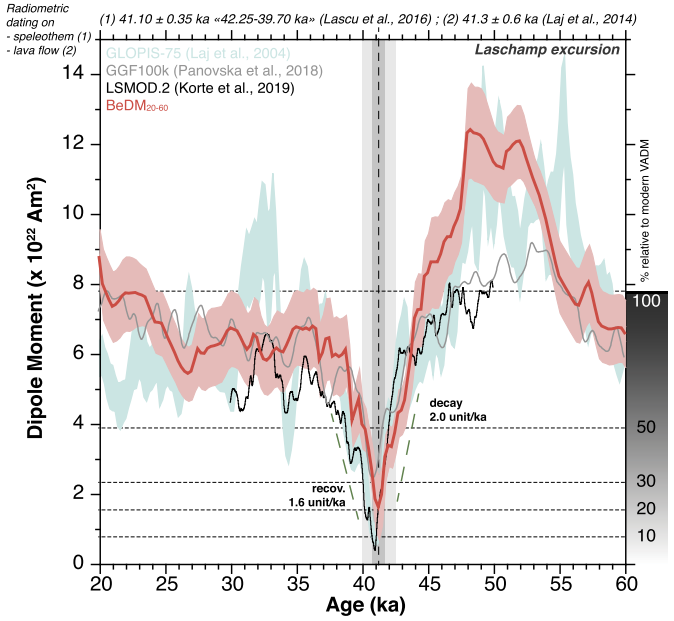

Fig. 6. Geomagnetic dipole moment dynamics over the 20–60 ka time interval and across the Laschamp excursion as seen from independent reconstructions based on calibrated global RPI stack: GLOPIS-75 (Laj et al., 2004); geomagnetic field models based on compilation of paleomagnetic sediment, archeomagnetic and/or lava flow records: GGF100k (Panovska et al., 2018) and LSMOD.2 (Korte et al., 2019); and calibrated marine Be ratio stacks: BeDM$_{20-60}$ (this study).

A slope break (with large standard deviation) between 47–45 ka, corresponds to a minor RPI low recorded in some RPI records and stacks (e.g. Stoner et al., 2002; Laj et., 2004; Channell et al., 2017) and reproduced by geomagnetic models (Panovska et al., 2018; Korte et al., 2019). This event is well expressed in the calibrated MarIce-Be stack containing the high-resolution ^{10}Be-flux record

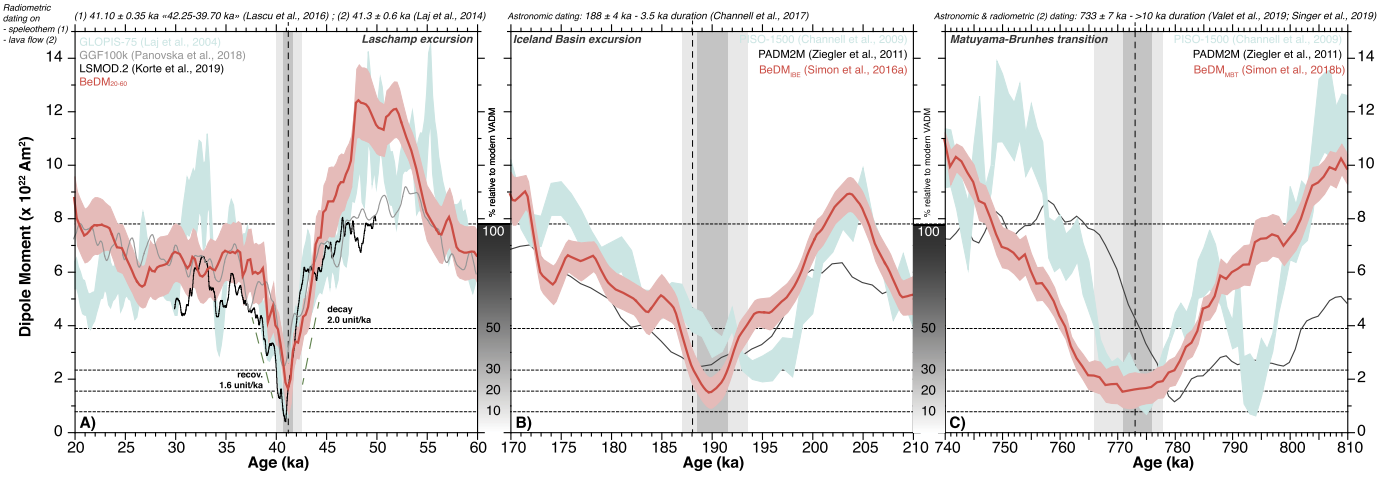

Fig. 7. Geomagnetic dipole moment dynamics across the Laschamp (A) and Iceland Basin (B) excursions, and Matuyama-Brunhes transition (C) as seen from independent reconstructions based on calibrated global RPI stacks: GLOPIS-75 (Laj et al., 2004) and PISO-1500 (Channell et al., 2009); geomagnetic field model based on a compilation of paleomagnetic sediment, archeomagnetic and/or lava flow records: GGF100k (Panovska et al., 2018), LSMOD.2 (Korte et al., 2019) and PADM2M (Ziegler et al., 2011); and calibrated marine Be ratio stacks (this study and Simon et al., 2016a, 2018b).

from Greenland Summit (Fig. S2C). From 44 to 41.3 ka, the dipole moment collapsed from 7.0 ± 0.9 down to $1.6 \pm 0.7 \times 10^{22}$ Am^2, with an average rate of -2.0×10^{22} Am^2/ka.

The weakest GDM phase lasted less than one millennium at most (41.6 to 40.9 ka), with an average GDM value of $1.8 \pm 0.7 \times 10^{22}$ Am^2, i.e. about 15–30% of present-day GDM value (Fig. 6). The age and duration are fully consistent with those deduced from various archives (e.g. Muscheler et al., 2005; Nowaczyk et al., 2012; Laj et al., 2014; Lascu et al., 2016; Channell et al., 2017). The average GDM value (± full uncertainty) obtained from the BeDM$_{20-60}$ is statistically similar to those recovered from absolute paleointensity measurements of transitional lava flows recording the Laschamp excursion, i.e. $1.6 \pm 0.3 \times 10^{22}$ Am^2 (Roperch et al., 1988) and $1.3 \pm 0.4 \times 10^{22}$ Am^2 (Laj et al., 2014). Such low dipole moment values are also reconstructed from transitional lava flows (e.g. Singer et al., 2019) and a BeDM record covering the Matuyama-Brunhes transition ($1.7 \pm 0.4 \times 10^{22}$ Am^2; Simon et al., 2018b), or computed by numerical dynamo simulations of reversals (Glatzmaier and Roberts, 1995; Buffett et al., 2013; Wicht and Meduri, 2016).

To further confront the GDM record of the Laschamp, we examine another well-known and frequently recorded geomagnetic excursion, the Iceland Basin Excursion (IBE; e.g. Channell, 2014). The Be ratio compilation of Simon et al. (2016a) was calibrated using the methods described in section 4, providing an average dipole moment value of $1.8 \pm 0.5 \times 10^{22}$ Am^2 over the IBE time interval (191.5–188.5 ka; Fig. 7B). This value is not significantly different from the VADM value $2.2 \pm 0.2 \times 10^{22}$ Am^2 obtained from absolute paleointensity measured on a transitional lava flow of the Unzen volcano (Japan) tentatively associated with the IBE (Yamamoto et al., 2010). At such weak GDM values the equilibrium (tipping-point) between the residual non-dipole field and an equatorial dipole can trigger either a short-lived geomagnetic excursion or a long-lived successful reversal (Valet et al., 2008). The three studied cases thus provide similar low GDM values lasting various durations. Setting an arbitrary GDM value threshold value at 2×10^{22} Am^2 (about 25% of the present-day dipole moment), the three different events (Laschamp, IBE and M/B full reversal) span durations of about 1 ka, 3 ka and more than 10 ka, respectively (Fig. 7). These durations are significantly different and likely express different mechanisms involved in the core fluid circulation leading to either failure or success of the reversal process.

Following the Laschamp excursion, the GDM increased at an average rate of 1.6×10^{22} Am^2/ka until reaching a plateau from 38.5 ka to 27.5 ka, where it slightly oscillates around relatively stable values of $6.3 \pm 0.3 \times 10^{22}$ Am^2 (average ± standard deviation; about 80% of the present GDM value). No significant GDM low appears around 34 ± 2 ka, age usually retained for the Mono Lake excursion (MLE) (e.g. Liddicoat and Coe, 1979; Negrini et al., 2014; Lund et al., 2017b; Jiabo et al., 2019). This observation suggests that the MLE may have been triggered by a non-dipole field pulse rather than by a significant dipole field collapse (e.g. models of Panovska et al., 2018; Korte et al., 2019), in contradiction with low RPI values and weak absolute PI records associated with the MLE observed from far sites distributed worldwide (e.g. Cassata et al., 2008; Kissel et al., 2011; Laj et al., 2014; Lund et al., 2017a; Channell, 2006; Jiabo et al., 2019). A limited GDM low ($5.4 \pm 0.7 \times 10^{22}$ Am^2) is recorded at 26.7 ka, a time of an excursional signature signaled from one single North Atlantic record (Channell et al., 2016). From 26.5 to 20 ka, the GDM increases up to $8.7 \pm 0.9 \times 10^{22}$ Am^2, i.e. just above the present-day dipole moment value. Overall, the BeDM$_{20-60}$ record does not support the occurrence of geomagnetic dipole-controlled excursions over the 20 ka time interval following the Laschamp.

The GDM loss rate reconstructed between 48 and 41 ka, i.e. prior to the Laschamp excursion, reached a maximum of 2.0×10^{22} Am^2/ka. It corresponds to those computed from high resolution calibrated-RPI records (Laj and Kissel, 2015), is identical to that computed prior to the Matuyama-Brunhes reversal from high-resolution Be ratio of the Chiba section (Simon et al., 2019) and indistinguishable from decreasing rates measured from archaeointensity records over the last three millennia (e.g. Genevey et al., 2008). This is about half of the decay rate of the axial dipole field observed over the last two centuries (Finlay et al., 2016), pointing out that the geomagnetic dipole field decayed faster during the last centuries than before excursions and reversals documented by paleomagnetic or cosmogenic ^{10}Be results.

9. Conclusion

We present new high-resolution Be ratio results from the equatorial core MD05-2920 located on the northern coast of Papua New Guinea. Together with previous paleomagnetic and Be ratio results (Ménabréaz et al., 2012; Simon et al., 2016a), these data provide an unprecedented resolution of 200 years over the 46–36 ka time interval and a "mean" resolution of 500 years over the 60–20 ka period. A significant Be ratio peak synchronized with the Laschamp excursion at 41 ka is recorded 18 cm above the corresponding

RPI minimum. This offset corresponds to a 1.6 ka lock-in delay due to post-depositional remanent magnetization (PDRM). When corrected to account for the lock-in depth, the Be ratio and RPI records present a rather similar asymmetric behavior before and after the dipole low, despite some apparent smearing of the paleomagnetic record. The new Be ratio data set is compiled with three other marine sequence records to construct the updated global record of ^{10}Be production variations across the Laschamp excursion. This compilation exhibits a high degree of coherence between data sets from low to mid latitudes and strong correlations with high latitude ^{10}Be-flux records, fully supporting the occurrence of a global atmospheric ^{10}Be production doubling event triggered by depleted magnetospheric shielding. The Be ratio stack was converted into geomagnetic dipole moment (GDM) values using two independent approaches: 1) a theoretical model and transfer function and, 2) a statistical calibration using selected absolute V(A)DM values drawn from absolute paleointensities measured on lava flows. Both methods provide similar results, presented here as a new Be ratio derived dipole moment ($BeDM_{20-60}$) record. We discuss the amplitude and dynamics of GDM variations across the Laschamp excursion: before 48 ka, the $BeDM_{20-60}$ record documents high field values ($> 11 \times 10^{22}$ Am^2), prior to a two-step decrease reaching the minimum value ($1.8 \pm 0.7 \times 10^{22}$ Am^2) between 41.6 and 40.9 ka. This value is consistent with the most reliable V(A)DM values of lava flows attributed to the Laschamp, Iceland-Basin excursion and Matuyama-Brunhes reversal. Following the Laschamp minimum, the field partly recovered showing an asymmetric behavior between a sharp decrease from high field values and slower recovery to mid field values ($\sim 6 \times 10^{22}$ Am^2). The $BeDM_{20-60}$ record documents only small-amplitude GDM variations in the 38–20 ka interval. This suggests that if excursions occurred (e.g. the Mono Lake excursion), they were not accompanied by durable and deep collapses of the dipole moment triggering significant cosmogenic ^{10}Be overproduction events.

Our approach provides an independent method to constrain paleomagnetic records, notably their reliability on recording accurate amplitude and rhythms of the dipole behavior, two prerequisites to stimulate discussion and prediction on geomagnetic field variations over the next millennia.

CRediT authorship contribution statement

Q.S., N.T. and D.L.B. initiated the study. Q.S. supervised the study and new measurements; compiled, processed, interpreted data and wrote the manuscript with the contribution of NT and DLB. All authors contributed to the discussion and edition of the manuscript.

Declaration of competing interest

The authors declare that they have no known competing financial interests or personal relationships that could have appeared to influence the work reported in this paper.

Acknowledgements

We acknowledge Sandrine Choy for beryllium sample preparation. Toshi Yamazaki and an anonymous reviewer are thanked for constructive and helpful comments. The ASTER AMS national facility (CEREGE, Aix en Provence) is supported by INSU/CNRS, IRD and by the ANR through the EQUIPEX "ASTER-CEREGE" action. This study was initiated by the ANR MAGORB project to NT (ANR 09 BLAN 0053) and was since 2015 supported by the ERC advanced grant to JPV "GA 339899-EDIFICE" under the ERC's 7th Framework Program (FP7-IDEA-ERC). The data presented in this study are available within the supporting information.

Appendix A. Supplementary material

Supplementary material related to this article can be found online at https://doi.org/10.1016/j.epsl.2020.116547.

References

Bard, E., Rostek, F., Ménot-Combes, G., 2004. Radiocarbon calibration beyond 20,000 ^{14}C yr B.P. by means of planktonic foraminifera of the Iberian Margin. Quat. Res. 61, 204–214.

Beer, J., Blinov, A., Bonani, G., Finkel, R.C., Hofmann, H.J., Lehmann, B., Oeschger, H., Sigg, A., Schwander, J., Staffelbach, T., Stauffer, B., Suter, M., Wötfli, W., 1990. Use of ^{10}Be in polar ice to trace the 11-year cycle of solar activity. Nature 347, 164–166.

Biggin, A.J., Paterson, G.A., 2014. A new set of qualitative reliability criteria to aid inferences on palaeomagnetic dipole moment variations through geological time. Front. Earth Sci. 2 (24). https://doi.org/10.3389/feart.2014.00024.

Biggin, A.J., Strik, G., Langereis, C.G., 2009. The intensity of the geomagnetic field in the late-Archaean: new measurements and an analysis of the updated IAGA palaeointensity database. Earth Planets Space 61 (1), 9–22.

Blanchet, C.L., Thouveny, N., de Garidel-Thoron, T., 2006. Evidence for multiple paleomagnetic intensity lows between 30 and 50 ka BP from a western equatorial Pacific sedimentary sequence. Quat. Sci. Rev. 25, 1039–1052.

Bonhommet, N., Babkine, J., 1967. Sur la presence d'aimantation inverse dans la Chaîne des Puys. C.R. Hebs. Seances Acad. Sci. Ser. B 264, 92–94.

Bourlès, D.L., Raisbeck, G.M., Yiou, F., 1989. ^{10}Be and ^{9}Be in Marine sediments and their potential for dating. Geochim. Cosmochim. Acta 53 (2), 443–452.

Braucher, R., Guillou, V., Bourlès, D.L., Arnold, M., Aumaître, G., Keddadouche, K., Nottoli, E., 2015. Preparation of ASTER in-house ^{10}Be/^{9}Be standard solutions. Nucl. Instrum. Methods Phys. Res., Sect. B, Beam Interact. Mater. Atoms 361, 335–340.

Bronk Ramsey, C., Heaton, T.J., Schlolaut, G., Staff, R.A., Bryant, C.L., Brauer, A., Lamb, H.F., Marshall, M.H., Nakagawa, T., 2020. Reanalysis of the atmospheric radiocarbon calibration record from lake Suigetso, Japan. Radiocarbon 62 (4), 1–11. https://doi.org/10.1017/RDC.2020.18.

Brown, M.C., Donadini, F., Korte, M., Nilsson, A., Korhonen, K., Lodge, A., Lengyel, S.N., Constable, C.G., 2015. GEOMAGIA50.v3: 1. General structure and modifications to the archeological and volcanic database. Earth Planets Space 67, 83. https://doi.org/10.1186/s40623-015-0232-0.

Brown, M.C., Korte, M., 2016. A simple model for geomagnetic field excursions and inferences for palaeomagnetic observations. Phys. Earth Planet. Inter. 254, 1–11.

Brown, M.C., Korte, M., Holme, R., Wardinski, I., Gunnarson, S., 2018. Earth's magnetic field is probably not reversing. Proc. Natl. Acad. Sci. USA 115 (20), 5111–5116.

Buffett, B., Ziegler, L., Constable, C.G., 2013. A stochastic model for palaeomagnetic field variations. Geophys. J. Int. 195, 86–97.

Carcaillet, J.T., Bourlès, D.L., Thouveny, N., 2004a. Geomagnetic dipole moment and ^{10}Be production rate intercalibration from authigenic ^{10}Be/^{9}Be for the last 1.3 Ma. Geochem. Geophys. Geosyst. 5, Q05006.

Carcaillet, J.T., Bourlès, D.L., Thouveny, N., Arnold, M., 2004b. A high resolution authigenic ^{10}Be/^{9}Be record of geomagnetic moment variations over the last 300 ka from sedimentary cores of the Portuguese margin. Earth Planet. Sci. Lett. 219 (3), 397–412.

Cassata, W.S., Singer, B.S., Cassidy, J., 2008. Laschamp and Mono Lake geomagnetic excursions recorded in New Zealand. Earth Planet. Sci. Lett. 268, 76–88.

Channell, J.E.T., 2006. Late Brunhes polarity excursions (Mono Lake, Laschamp, Iceland basin and Pringle falls) recorded at ODP Site 919 (Irminger Basin). Earth Planet. Sci. Lett. 244, 378–393.

Channell, J.E.T., 2014. The Iceland basin excursion: age duration, and excursion field geometry. Geochem. Geophys. Geosyst. 15, 4920–4935. https://doi.org/10.1002/2014GC005564.

Channell, J.E.T., Xuan, C., Hodell, D.A., 2009. Stacking paleointensity and oxygen isotope data for the last 1.5 Myr (PISO-1500). Earth Planet. Sci. Lett. 283 (1–4), 14–23. https://doi.org/10.1016/j.epsl.2009.03.012.

Channell, J.E.T., Harrison, R.J., Lascu, I., McCave, I.N., Hibbert, F.D., Austin, W.E.N., 2016. Magnetic record of deglaciation using FORC-PCA, sortable-silt grain size, and magnetic excursion at 26 ka, from the Rockall trough (NE Atlantic). Geochem. Geophys. Geosyst. 17, 1823–1841.

Channell, J.E.T., Vasquez Riveiros, N., Gottschalk, J., Waelbroeck, C., Skinner, L.C., 2017. Age and duration of Laschamp and Iceland basin geomagnetic excursions in the South Atlantic Ocean. Quat. Sci. Rev. 167, 1–13.

Channell, J.E.T., Singer, B.S., Jicha, B.R., 2020. Timing of quaternary geomagnetic reversals and excursions in volcanic and sedimentary archives. Quat. Sci. Rev. 228, 106114.

Chmeleff, J., von Blanckenburg, F, Kossert, K., Jakob, D., 2010. Determination of the ^{10}Be half-life by multicollector ICP-MS and liquid scintillation counting. Nucl. Instrum. Methods Phys. Res., Sect. B, Beam Interact. Mater. Atoms 268 (2), 192–199.

Christl, M., Lippold, J., Steinhilber, F., Bernsdorff, F., Mangini, A., 2010. Reconstruction of global ^{10}Be production over the past 250 ka from highly accumulating Atlantic drift sediments. Quat. Sci. Rev. 29 (19–20), 2663–2672. https://doi.org/10.1016/j.quascirev.2010.06.017.

Coe, R.S., Liddicoat, J.C., 1994. Overprinting of natural magnetic remanence in lake sediments by a subsequent high-intensity field. Nature 367, 57–59.

Egli, R., Zhao, X., 2015. Natural remanent magnetization acquisition in bioturbated sediment: general theory and implications for relative paleointensity reconstructions. Geochem. Geophys. Geosyst. 16, 995–1016.

Elsasser, W., Ney, E.P., Winckler, J.R., 1956. Cosmic-ray intensity and geomagnetism. Nature 178, 1226–1227.

Finlay, C.C., Aubert, J., Gillet, N., 2016. Gyre-driven decay of the Earth's magnetic dipole. Nat. Commun. 7, 10422.

Frank, M., Schwarz, B., Baumann, S., Kubik, P.W., Suter, M., Mangini, A., 1997. A 200 kyr record of cosmogenic radionuclide production rate and geomagnetic field intensity from ^{10}Be in globally stacked deep-sea sediments. Earth Planet. Sci. Lett. 149 (1–4), 121–129.

Genevey, A., Gallet, Y., Constable, C.G., Korte, M., Hulot, G., 2008. ArcheoInt: an upgraded compilation of geomagnetic field intensity data for the past ten millennia and its application to the recovery of the past dipole moment. Geochem. Geophys. Geosyst. 9, Q04038.

Glatzmaier, G.A., Roberts, P.H., 1995. A three-dimensional self-consistent computer simulation of a geomagnetic field reversal. Nature 377, 203–209.

Heikkilä, U., Beer, J., Feichter, J., 2009. Meridional transport and deposition of atmospheric ^{10}Be. Atmos. Chem. Phys. 9, 515–527.

Horiuchi, K., Kamata, K., Maejima, S., Sasaki, S., Sasaki, N., Yamazaki, T., Fujita, S., Motoyama, H., Matsuzaki, H., 2016. Multiple ^{10}Be records revealing the history of cosmic-ray variations across the Iceland basin excursion. Earth Planet. Sci. Lett. 440, 105–114.

Hyodo, M., 1984. Possibility of reconstruction of the past geomagnetic field from homogeneous sediments. J. Geomagn. Geoelectr. 36, 45–62.

Ingham, E., Turner, G.M., Conway, C.E., Heslop, D., Roberts, A.P., Leonard, G., Townsend, D., Calvert, A., 2017. Volcanic records of the Laschamp geomagnetic excursion from Mt Ruapehu, New Zealand. Earth Planet. Sci. Lett. 472, 131–141.

Jiabo, L., Nowaczyk, N., Frank., U., 2019. Geomagnetic paleosecular variation record spanning from 40 to 20 ka – implications for the Mono Lake excursion from Black Sea sediments. Earth Planet. Sci. Lett. 509, 114–124.

Kissel, C., Guillou, H., Laj, C., Carracedo, J.C., Nomade, S., Perez-Torrado, F., Wandres, C., 2011. The Mono Lake excursion recorded in phonolitic lavas from Tenerife (Canary Islands): paleomagnetic analyses and coupled K/Ar and Ar/Ar dating. Phys. Earth Planet. Inter. 187, 232–244.

Knudsen, M.F., Riisager, P., Donadini, F., Snowball, I., Muscheler, R., Korhonen, K., Pesonen, L.J., Jacobsen, B.H., 2008. Variations in the geomagnetic dipole moment during the Holocene and the past 50 kyr. Earth Planet. Sci. Lett. 272, 319–329.

Korschinek, G., Bergmaier, A., Faestermann, T., Gerstmann, U.C., Knie, K., Rugel, G., Wallner, A., Dillmann, I., Dollinger, G., Lierse von Gostomski, Ch., Kossert, K., Maiti, M., Poutivtsev, M., Remmert, A., 2010. A new value for the half-life of ^{10}Be by heavy-ion elastic recoil detection and liquid scintillation counting. Nucl. Instrum. Methods Phys. Res. B 268 (2), 187–191.

Korte, M., Constable, C., Donadini, F., Holme, R., 2011. Reconstructing the Holocene geomagnetic field. Earth Planet. Sci. Lett. 312, 497–505.

Korte, M., Brown, M.C., Panovska, S., Wardinski, I., 2019. Robust characteristics of the Laschamp and Mono Lake geomagnetic excursions: results from global field models. Front. Earth Sci. 7, 86.

Laj, C., Channell, J.E.T., 2015. Geomagnetic excursions, second edition. In: Treatise on Geophysics. In: Geomagnetism, vol. 5. Elsevier, Amsterdam, pp. 343–383. Chapter 10.

Laj, C., Kissel, C., 2015. An impending geomagnetic transition? Hints from the past. Front. Earth Sci. 3, 61.

Laj, C., Kissel, C., Beer, J., 2004. High Resolution Global Paleointensity Stack Since 75 Kyrs (GLOPIS-75) Calibrated to Absolute Values. Timescales of the Geomagnetic Field, vol. 145. AGU Monograph, Washington, pp. 255–265.

Laj, C., Guillou, H., Kissel, C., 2014. Dynamics of the earth magnetic field in the 10-75 kyr period comprising the Laschamp and Mono Lake excursions: new results from the French Chaîne des Puys in a global perspective. Earth Planet. Sci. Lett. 387, 184–197.

Lal, D., Peters, B., 1967. Cosmic Ray Produced Radioactivity on the Earth. Handbuch der Physik, vol. XLVI/2. Springer, New York, pp. 551–612.

Lascu, I., Feinberg, J.M., Dorale, J.A., Cheng, H., Edwards, R.L., 2016. Age of the Laschamp excursion determined by U-Th dating of a speleothem geomagnetic record from North America. Geology 44, 139–142.

Leonhardt, R., Fabian, K., Winklhofer, M., Ferk, A., Laj, C., Kissel, C., 2009. Geomagnetic field evolution during the Laschamp excursion. Earth Planet. Sci. Lett. 278, 87–95.

Liddicoat, J., Coe, R., 1979. Mono Lake geomagnetic excursion. J. Geophys. Res. 84, 261–271.

Lingenfelter, R.E., 1963. Production of carbon 14 by cosmic-ray neutrons. Rev. Geophys. 1 (1), 35–55.

Lisiecki, L.E., Raymo, M.E., 2005. A Pliocene–Pleistocene stack of 57 globally distributed benthic δ^{18}O record. Paleoceanography 20, PA1003. https://doi.org/10.1029/2004PA001071.

Løvlie, R., 1976. The intensity pattern of post-depositional remanence acquired in some marine sediments deposited during a reversal of the external magnetic field. Earth Planet. Sci. Lett. 30, 209–214.

Lund, S., Schwartz, M., Stott, L., 2017a. Long-term palaeomagnetic secular variation and excursions from the western equatorial Pacific Ocean (MIS2-4). Geophys. J. Int. 209, 587–596.

Lund, S., Benson, L., Negrini, R., Liddicoat, J., Mensing, S., 2017b. A full-vector paleomagnetic secular variation record (PSV) from Pyramid Lake (Nevada) from 47-17 ka: evidence for the successive Mono Lake and Laschamp excursions. Earth Planet. Sci. Lett. 458, 120–129.

Lund, S.P., Schwartz, M., Keigwin, L., Johnson, T., 2005. Deep-sea sediment records of the Laschamp geomagnetic field excursion (41,000 calendar years before present). J. Geophys. Res. 110, B04101. https://doi.org/10.1029/2003JB002943.

Mazaud, A., Sicre, M.A., Ezat, U., Pichon, J.J., Duprat, J., Laj, C., Kissel, C., Beaufort, L., Michel, E., Turon, J.L., 2002. Geomagnetic assisted stratigraphy and SST changes in core MD94–103 (southern Indian Ocean): possible implications for North-South climatic relationships around H4. Earth Planet. Sci. Lett. 201, 159–170.

Ménabréaz, L., Thouveny, N., Bourlès, D.L., Deschamps, P., Hamelin, B., Demory, F., 2011. The Laschamp geomagnetic dipole low expressed as a cosmogenic ^{10}Be atmospheric overproduction at ~41 ka. Earth Planet. Sci. Lett. 312 (3–4), 305–317.

Ménabréaz, L., Bourlès, D.L., Thouveny, N., 2012. Amplitude and timing of the Laschamp geomagnetic dipole low from the global atmospheric ^{10}Be overproduction: contribution of authigenic ^{10}Be/^{9}Be ratios in west equatorial Pacific sediments. J. Geophys. Res. 117, B11101.

Ménabréaz, L., Thouveny, N., Bourlès, D.L., Vidal, L., 2014. The geomagnetic dipole moment variation between 250 and 800 ka BP reconstructed from the authigenic ^{10}Be/^{9}Be signature in West Equatorial Pacific sediments. Earth Planet. Sci. Lett. 385, 190–205. https://doi.org/10.1016/j.epsl.2013.10.037.

Mochizuki, N., Tsunakawa, H., Shibuya, H., Cassidy, J., Smith, I.E.M., 2006. Palaeointensities of the Auckland geomagnetic excursions by the LTD-DHT Shaw method. Phys. Earth Planet. Inter. 154, 168–179.

Muscheler, R., Beer, J., Kubik, P.W., Synal, H.A., 2005. Geomagnetic field intensity during the last 60,000 years based on ^{10}Be and ^{36}Cl from the Summit ice cores and ^{14}C. Quat. Sci. Rev. 24, 1849–1860.

Negrini, R.M., McCuan, D.T., Horton, R.A., Lopez, J.D., Cassata, W.S., Channell, J.E.T., Verosub, K.L., Knott, J.R., Coe, R.S., Liddicoat, J.C., Lund, S.P., Benson, L.V., Sarna-Wojcicki, A.M., 2014. Nongeocentric axial dipole field behavior during the Mono Lake excursion. J. Geophys. Res., Solid Earth 119, 2567–2581. https://doi.org/10.1002/2013JB010846.

Nilsson, A., Muscheler, R., Snowball, I., Aldahan, A., Possnert, G., Augustinus, P., Atkin, D., Stephens, T., 2011. Multi-proxy identification of the Laschamp geomagnetic field excursion in Lake Pupuke, New Zealand. Earth Planet. Sci. Lett. 311, 155–164.

Nilsson, A., Suttie, N., Hill, M.J., 2018. Short-term magnetic field variations from the post-depositional remanence of Lake sediments. Front. Earth Sci. 6, 39.

Nowaczyk, N.R., Arz, H.W., Frank, U., Kind, J., Plessen, B., 2012. Dynamics of the Laschamp geomagnetic excursion from Black Sea sediments. Earth Planet. Sci. Lett. 351–352, 54–69.

O'Brien, K., 1979. Secular variations in the production of cosmogenic isotopes in the Earth's atmosphere. J. Geophys. Res. 84 (A2), 423–431.

Panovska, S., Constable, S.G., Korte, M., 2018. Extending global continuous geomagnetic field reconstructions on timescales beyond human civilization. Geochem. Geophys. Geosyst. 19.

Pavón-Carrasco, F.J., Osete, M.L., Torta, J.M., De Santis, A., 2014. A geomagnetic field model for the Holocene based on archeomagnetic and lava flow data. Earth Planet. Sci. Lett. 388, 98–109.

Poluianov, S.V., Kovaltsov, G.A., Mishev, A.L., Usoskin, I.G., 2016. Production of cosmogenic isotopes ^{7}Be, ^{10}Be, ^{14}C, ^{22}Na, and ^{36}Cl in the atmosphere: altitudinal profiles of yield functions. J. Geophys. Res., Atmos. 121, 8125–8136.

Raisbeck, G.M., Yiou, F., Bourlès, D., Kent, D.V., 1985. Evidence for an increase in cosmogenic ^{10}Be during a geomagnetic reversal. Nature 315, 315–317.

Raisbeck, G.M., Yiou, F., Bourlès, D.L., Lorius, C., Jouzel, J., Barkov, N.I., 1987. Evidence for two intervals of enhanced ^{10}Be deposition in Antarctic ice during the last glacial period. Nature 326, 273–277.

Raisbeck, G.M., Cauquoin, A., Jouzel, J., Landais, A., Petit, J.-R., Lipenkov, V.Y., Beer, J., Synal, H.-A., Oerter, H., Johnsen, S.J., Steffensen, J.P., Svensson, A., Yiou, F., 2017. An improved North–South synchronization of ice core records around the 41 kyr ^{10}Be peak. Clim. Past 13, 217–229.

Roberts, A.P., 2008. Geomagnetic excursions: knowns and unknowns. Geophys. Res. Lett. 35, L17307.

Roberts, A.P., Winklhofer, M., 2004. Why are geomagnetic excursions not always recorded in sediments? Constraints from post-depositional remanent magnetization lock-in modelling. Earth Planet. Sci. Lett. 227, 345–359.

Roberts, A.P., Tauxe, L., Heslop, D., 2013. Magnetic paleointensity stratigraphy and high-resolution quaternary geochronology: successes and future challenges. Quat. Sci. Rev. 61, 1–16.

Roperch, P., Bonhommet, N., Levi, S., 1988. Paleointensity of the Earth's magnetic field during the Laschamp excursion and its geomagnetic implications. Earth Planet. Sci. Lett. 88, 209–219.

Sagnotti, L., Budillon, F., Dinarès-Turell, J., Iorio, M., Macri, P., 2005. Evidence for a variable paleomagnetic lock-in depth in the Holocene sequence from the

Salerno Gulf (Italy): implications for "high-resolution" paleomagnetic dating. Geochem. Geophys. Geosyst. 6, Q11013. https://doi.org/10.1029/2005GC001043.
Shackleton, N.J., Hall, M., Vincent, E., 2000. Phase relationship between millennial scale events 64,000-24,000 years ago. Paleoceanography 15, 565–569.
Shackleton, N.J., Fairbanks, R.G., Chiu, T.-C., Parrenin, F., 2004. Absolute calibration of the Greenland time scale: implications for Antarctic time scales and for $\delta^{14}C$. Quat. Sci. Rev. 23, 1513–1522.
Simon, Q., Thouveny, N., Bourlès, D.L., Nuttin, L., St-Onge, G., Hillaire-Marcel, C., 2016b. Authigenic $^{10}Be/^{9}Be$ ratios and ^{10}Be-fluxes ($^{230}Th_{xs}$-normalized) in central Baffin Bay during the last glacial cycle: paleoenvironmental implications. Quat. Sci. Rev. 140, 142–162.
Simon, Q., Thouveny, N., Bourlès, D.L., Valet, J.-P., Bassinot, F., Ménabréaz, L., Guillou, V., Choy, S., Beaufort, L., 2016a. Authigenic $^{10}Be/^{9}Be$ ratio signatures of the cosmogenic nuclide production linked to geomagnetic dipole moment variation since the Brunhes/Matuyama boundary. J. Geophys. Res. 121, 7716–7741.
Simon, Q., Bourlès, D.L., Thouveny, N., Horng, C.-S., Valet, J.-P., Bassinot, F., Choy, S., 2018a. Cosmogenic signature of geomagnetic reversals and excursions from the Réunion event to the Matuyama–Brunhes transition (0.7–2.14 Ma interval). Earth Planet. Sci. Lett. 482, 510–524. https://doi.org/10.1016/j.epsl.2017.11.021.
Simon, Q., Thouveny, N., Bourlès, D.L., Bassinot, F., Savranskaia, T., Valet, J.-P., 2018b. Increased production of cosmogenic ^{10}Be recorded in oceanic sediment sequences: information on the age, duration, and amplitude of the geomagnetic dipole moment minimum over the Matuyama–Brunhes transition. Earth Planet. Sci. Lett. 489, 191–202.
Simon, Q., Suganuma, Y., Okada, M., Haneda, Y., ASTER Team, 2019. High-resolution ^{10}Be and paleomagnetic recording of the last polarity reversal in the Chiba composite section: age and dynamics of the Matuyama-Brunhes transition. Earth Planet. Sci. Lett. 519, 92–100.
Singer, B.S., Jicha, B.R., Mochizuki, N., Coe, R.S., 2019. Synchronizing volcanic, sedimentary, and ice core records of Earth's last magnetic polarity reversal. Sci. Adv. 5, eaaw4621.
Staff, R.A., Hardiman, M., Bronk Ramsey, C., Adolphi, F., Hare, V.J., Koutsodendris, A., Pross, J., 2019. Reconciling the Greenland ice-core and radiocarbon timescales through the Laschamp geomagnetic excursion. Earth Planet. Sci. Lett. 520, 1–9.
Stoner, J.S., Laj, C., Channell, J.E.T., Kissel, C., 2002. South Atlantic and North Atlantic geomagnetic paleointensity stacks (0–80 ka): implications for inter-hemispheric correlation. Quat. Sci. Rev. 21, 1141–1151.
Stoner, J.S., St-Onge, G., 2007. Magnetic stratigraphy in paleoceanography: reversals, excursions, paleointensity and secular variation. In: Hillaire-Marcel, C., de Vernal, A. (Eds.), Developments in Marine Geology, vol. 1, Proxies in Late Cenozoic Paleoceanography. Elsevier, Amsterdam, pp. 99–138.
Suganuma, Y., Okuno, J., Heslop, D., Roberts, A.P., Yamazaki, T., Yokoyama, Y., 2011. Post-depositional remanent magnetization lock-in for marine sediments deduced from ^{10}Be and paleomagnetic records through the Matuyama-Brunhes boundary. Earth Planet. Sci. Lett. 311, 39–52.
Tachikawa, K., Cartapanis, O., Vidal, L., Beaufort, L., Barlyaeva, T., Bard, E., 2011. The precession phase of hydrological variability in the Western Pacific Warm Pool during the past 400 ka. Quat. Sci. Rev. 30, 3716–3727.
Thouveny, N., Creer, K.M., Blunk, I., 1990. Extension of the Lac du Bouchet palaeomagnetic record over the last 120,000 years. Earth Planet. Sci. Lett. 97, 140–161.
Thouveny, N., Creer, K.M., Williamson, D., 1993. Geomagnetic moment variations in the last 70,000 years, impact on production of cosmogenic isotopes. Glob. Planet. Change 7, 157–172.
Thouveny, N., Carcaillet, J., Moreno, E., Leduc, G., Nerini, D., 2004. Geomagnetic moment variation and paleomagnetic excursions since 400 kyr BP; a stacked record from sedimentary sequences of the Portuguese margin. Earth Planet. Sci. Lett. 219, 377–396.
Valet, J.P., Plenier, G., 2008. Simulations of a time-varying non dipole field during geomagnetic reversals and excursions. Phys. Earth Planet. Inter. 169 (1–4), 178–193.
Valet, J.P., Plenier, G., Herrero-Berva, E., 2008. Geomagnetic excursions reflect an aborted polarity state. Earth Planet. Sci. Lett. 274, 472–478.
Valet, J.P., Meynadier, L., Simon, Q., Thouveny, N., 2016. When and why sediments fail to record the geomagnetic field during polarity reversals. Earth Planet. Sci. Lett. 453, 96–107.
Valet, J.P., Tanty, C., Carlut, J., 2017. Detrital magnetization of laboratory-redeposited sediments. Geophys. J. Int. 210, 34–41.
Valet, J.P., Bassinot, F., Simon, Q., Savranskaia, T., Thouveny, N., Bourlès, D.L., Villedieu, A., 2019. Constraining the age of the last geomagnetic reversal from geochemical and magnetic analyses of Atlantic, Indian, and Pacific Ocean sediments. Earth Planet. Sci. Lett. 506, 323–331.
Vlag, P., Thouveny, N., Williamson, D., Rochette, P., Ben-Atig, F., 1996. Evidence for a geomagnetic excursion recorded in the sediments of Lac St. Front, France: a link with the Laschamp excursion? J. Geophys. Res. 101 (B12), 28,211–228,230.
Vlag, P., Thouveny, N., Rochette, P., 1997. Synthetic and sedimentary records of geomagnetic excursions. Geophys. Res. Lett. 24 (6), 723–726.
von Blanckenburg, F., Igel, H., 1999. Lateral mixing and advection of reactive isotope tracers in ocean basins: observations and mechanisms. Earth Planet. Sci. Lett. 169, 113–128.
Wicht, J., Meduri, D.G., 2016. A Gaussian model for simulated geomagnetic field reversals. Phys. Earth Planet. Inter. 259, 45–60.
Yamamoto, Y., Shibuya, H., Tanaka, H., Hoshizumi, H., 2010. Geomagnetic paleo- intensity deduced for the last 300 kyr from Unzen Volcano, Japan, and the dipolar nature of the Iceland basin excursion. Earth Planet. Sci. Lett. 293, 236–249.
Ziegler, L.B., Constable, C.G., Johnson, C.L., Tauxe, L., 2011. PADM2M: a penalized maximum likelihood model of the 0–2 Ma palaeomagnetic axial dipole moment. Geophys. J. Int. 184, 1069–1089.